AIP | APL Materials

Research Update: Photoelectrochemical water splitting and photocatalytic hydrogen production using ferrites (MFe_2O_4) under visible light irradiation

Ralf Dillert, Dereje H. Taffa, Michael Wark, Thomas Bredow, and Detlef W. Bahnemann

Citation: APL Mater. **3**, 104001 (2015); doi: 10.1063/1.4931763
View online: http://dx.doi.org/10.1063/1.4931763
View Table of Contents: http://scitation.aip.org/content/aip/journal/aplmater/3/10?ver=pdfcov
Published by the AIP Publishing

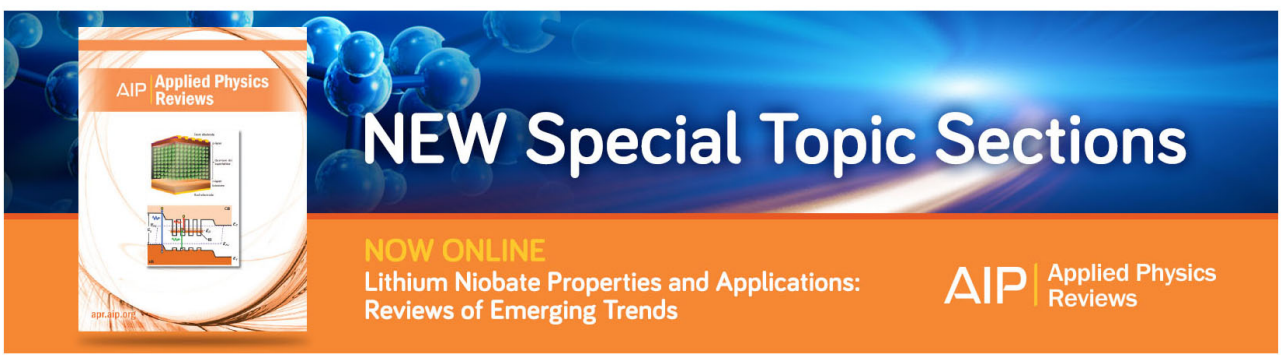

Research Update: Photoelectrochemical water splitting and photocatalytic hydrogen production using ferrites (MFe_2O_4) under visible light irradiation

Ralf Dillert,[1,2] Dereje H. Taffa,[3] Michael Wark,[3] Thomas Bredow,[4] and Detlef W. Bahnemann[1,5]

[1]*Institut für Technische Chemie, Gottfried Wilhelm Leibniz Universität Hannover, Callinstr. 3, 30167 Hannover, Germany*
[2]*Laboratorium für Nano- und Quantenengineering, Gottfried Wilhelm Leibniz Universität Hannover, Schneiderberg 39, 30167 Hannover, Germany*
[3]*Institut für Chemie, Technische Chemie, Carl-von-Ossietzky Universität Oldenburg, Carl-von-Ossietzky Str. 9-11, 26129 Oldenburg, Germany*
[4]*Mulliken Center for Theoretical Chemistry, Institut für Physikalische und Theoretische Chemie, Universität Bonn, Beringstraße 4, 53115 Bonn, Germany*
[5]*Laboratory for Nanocomposite Materials, Department of Photonics, Faculty of Physics, Saint-Petersburg State University, Ulianovskaia Str. 3, Peterhof, Saint-Petersburg 198504, Russia*

(Received 5 August 2015; accepted 15 September 2015; published online 25 September 2015)

The utilization of solar light for the photoelectrochemical and photocatalytic production of molecular hydrogen from water is a scientific and technical challenge. Semiconductors with suitable properties to promote solar-driven water splitting are a desideratum. A hitherto rarely investigated group of semiconductors are ferrites with the empirical formula MFe_2O_4 and related compounds. This contribution summarizes the published results of the experimental investigations on the photoelectrochemical and photocatalytic properties of these compounds. It will be shown that the potential of this group of compounds in regard to the production of solar hydrogen has not been fully explored yet. [http://dx.doi.org/10.1063/1.4931763]

Molecular hydrogen is considered as a substitute of fossil fuels but its solar powered production from water remains a challenge. By direct thermochemical splitting of water, an appreciable quantity of molecular hydrogen is only obtained in solar concentrators at temperatures exceeding 2500 K; in the presence of suitable catalysts, the temperature required for thermal water splitting can be decreased to about 1000 K.[1–3] The conversion of solar energy into molecular hydrogen under milder operating conditions demands photoelectrochemical or photocatalytic processes.[4–17] Numerous inorganic compounds from a variety of material classes have been studied in regard to their suitability as electrode materials and photocatalysts.[4,8,12,14–18] One of these classes are ferrites with the general empirical formula $M^1{}_xM^2{}_yFe_{3-x-y}O_4$. These ferrites have been employed as photocatalysts to form molecular hydrogen and/or oxygen from aqueous suspensions usually containing a sacrificial reagent as well as electrodes to investigate their potential use as photocathodes or photoanodes. To ensure direct comparison, all electrochemical potentials are given herein with respect to the normal hydrogen electrode (NHE).

Most of the ferrites with the empirical formula MFe_2O_4 (i.e., $M^1{}_xM^2{}_yFe_{3-x-y}O_4$, with $x = 1$ and $y = 0$) crystallize in the spinel structure. In the spinel ferrites, the oxide anions are arranged in a cubic close-packed lattice and the cations M and Fe occupy some or all of the octahedral and tetrahedral sites. Although the charges of M and Fe in the prototypical spinel structure ($x = 1$) are +2 and +3, respectively, other combinations are also possible.

Simple spinels of the type MFe_2O_4 can be regarded as compounds where the iron ions of the spinel magnetite, $^T[Fe]^O[Fe_2]O_4$, are substituted by other metal ions according to $^T[M_{1-y}Fe_y]^O[M_yFe_{2-y}]O_4$ where the superscripts ^{T} and ^{O} identify the tetrahedral and octahedral sites, respectively, and y

corresponds to the degree of inversion ($0 \leq y \leq 1$). Spinel compounds with the empirical formula $^{T}[M]^{O}[Fe_2]O_4$ ($y = 0$) are called normal ferrite spinels, while compounds with $^{T}[Fe]^{O}[MFe]O_4$ ($y = 1$) are inverse ferrite spinels.

Some compounds such as $MgFe_2O_4$, $CaFe_2O_4$, and $BaFe_2O_4$ are known to form orthorhombic phases.[19–21] Other ferrites such as $CuFe_2O_4$ form crystalline solids with cubic or tetragonal unit cells depending on the synthetic conditions.[22]

Ferrites are regarded to be chemically and thermally stable in aqueous systems.[23] Most of them are semiconductors with bandgap energies allowing the excitation by visible light, and energetic positions of the conduction and the valence bands are suitable for either reduction of protons and/or oxidation of water. The bandgap energies E_g as well as the energetic positions of the valence band E_{VB} and the conduction band E_{CB} of some simple ferrites are tabulated in Table I. The variation of M^1, M^2, x, and y in $M^1{}_xM^2{}_yFe_{3-x-y}O_4$ is known to affect the resistivity (conductivity),[24–29] the optical properties (reflectivity, bandgap energy),[24–29] and the *p*-/*n*-type behavior[30,31] of the semiconductor. Also, the ability to catalyze thermal reactions is affected by the chemical nature and the amount of M present in a $M_xFe_{3-x}O_4$ compound.[32–35]

Fundamental (photo)electrochemical investigations of ferrite electrodes such as Fe_3O_4,[36] $Li_{0.5}Fe_{2.5}O_4$,[37,38] $MgFe_2O_4$,[37–40] *p*-$CaFe_2O_4$,[41–49] $Ti_xFe_{3-x}O_4$,[50] *p*- and *n*-type $Co_xFe_{3-x}O_4$ and $CoTi_xFe_{2-x}O_4$,[30] *p*-$CoFe_2O_4$,[51] *p*- and *n*-type $NiFe_2O_4$,[31,52] *n*-$ZnFe_2O_4$,[24,37,38,48,53,54] $Zn_xTi_yFe_{3-x-y}O_4$,[24] and $CdFe_2O_4$[55] have been published. The results of these studies as they relate to the determination of the flatband potentials and the energetic positions of the valance and conduction bands of the semiconductors are as well summarized in Table I.

As becomes obvious from Table I, several cubic and orthorhombic ferrites show *p*-type conductivity. Consequently, these compounds are suitable to act as photocathodes for the hydrogen evolution reaction (HER) in cells being designed for photoelectrochemical water splitting. Although there is a great scientific and technical interest in photocathodes, only *p*-type $CaFe_2O_4$, $CoFe_2O_4$, and $NiFe_2O_4$ have been installed in photoelectrochemical cells (PECs) yet.

TABLE I. Bandgap energies and energetic positions of the bands of some selected MFe_2O_4 compounds.

M	Structure	Type	E_g/eV[a]	E_{VB}/V[b]	E_{CB}/V[b]	E_{fb}/V[b]	Remarks[c]	References
Fe	Spinel (magnetite)		~2.15			−0.12		36
Mg	Spinel	*n*	2.0	+1.38	−0.62		S, pH 7	56
Mg	Spinel	*p*	1.74_d	−0.38	−2.12	−0.27	E, NaOH (~pH 10)	40
Ca			1.9	+1.3	−0.6		E	41–43
Ca	Orthorhombic	*p*	1.94	+1.27	−0.66		S, pH 7	56 and 57
Ba	Orthorhombic		1.85–1.90					58
Co	Inverse spinel		$1.39 \pm 0.31_i$, $2.31 \pm 0.28_d$					59
Ni	Inverse spinel		$1.52 \pm 0.08_i$, 2.3_d, 2.74_d					59
Ni	Inverse spinel	*p*	1.56_d, 1.99_i	+0.18	−1.38	+0.06	E, 0.1M KCl	52
Cu						+0.36	E, 1M KOH	60
Cu	Tetragonal	*p*	1.42	+0.45	−0.97	+0.24	E, 0.2M KOH	61
Cu	Inverse spinel	*p*	1.54_i, 1.96_d	+0.26	−1.28	+0.11	E	22
Zn	Spinel					~(−0.26)	E, 1M NaOH	38
Zn			1.9			−0.41	E	24
Zn	Spinel	*n*	1.90	+1.75	−0.15		S, pH 7	62
Zn	Spinel	*p*	1.92_i	+0.62	−1.30	+0.42	E, 0.5M NaOH	63
Zn	Spinel	*n*				−0.04	E, 1M NaOH (pH 13.6)	53
Zn	Spinel		1.83_i, 1.93_d	+1.40	−0.53		E, 1M NaOH;	64
			1.81_i, 1.90_d	+1.65	−0.25		depending on synthetic method	
Cd			2.3			~0	E, 0.2M NaOH (pH 13.3)	55

[a]The values of the indirect and direct bandgaps are labeled by i and d, respectively.
[b]All values are given *vs*. NHE; if necessary, the values given in the reference have been converted.
[c]Determined by electrochemical measurement in suspension, S, or at an electrode, E.

Ye and co-workers have investigated the visible light induced water splitting reaction employing a |Pt|Na_2SO_4 (0.1M) |*p*-$CaFe_2O_4$| PEC.[47] The photocathodes have been fabricated by depositing $CaFe_2O_4$ thin films on fluorine-doped tin oxide (FTO) coated glass employing a pulsed laser deposition method. A hydrogen evolution rate of ~4.8 μmol m^{-2} h^{-1} was observed under visible light irradiation (300 W Xe) without applying any additional bias. In a three-electrode configuration, a cathodic photocurrent was observed at values more negative than +0.64 V. A photocurrent density of −117 μA cm^{-2} at −0.06 V was reported being significantly larger than the values reported by Matsumoto *et al.*[41,42] for metal-loaded $CaFe_2O_4$ photoelectrodes probably due to shorter electron transfer distances in the thinner films used in the work of Ye and co-workers and to their higher electric conductivity.[47]

Furthermore, Ye and co-workers have compared the photoelectrochemical properties of *p*-$CaFe_2O_4$, *n*-$ZnFe_2O_4$, *p*-$CaFe_2O_4$/*n*-$ZnFe_2O_4$, and multiple *p*-*n*-junction $CaFe_2O_4$/$ZnFe_2O_4$ photoelectrodes. The electrodes have been prepared by a pulsed laser deposition method using $CaFe_2O_4$ and $ZnFe_2O_4$ pellets as the targets and FTO as the substrate. The authors observed a photocathodic current assigned to the reduction of water on a single-layer *p*-$CaFe_2O_4$ thin film and a photoanodic current due to the oxidization of water on a single-layer *n*-$ZnFe_2O_4$ thin film. A FTO/$ZnFe_2O_4$/$CaFe_2O_4$ photoelectrode exhibited a negative photocurrent and a positive open circuit photovoltage (+0.025 V, λ = 430 nm, 118 μW cm^{-2}) indicating that this electrode with a *p*-$CaFe_2O_4$ layer at the surface contacting the electrolyte acts as a photocathode. Investigating the photoelectrochemical properties of four multiple-junction FTO/$(ZnFe_2O_4/CaFe_2O_4)_x$ photoelectrodes with the same single-layer thickness of 10–15 nm but an increasing number x (x = 10, 15, 20, and 25), a remarkable effect on the photocurrent density and the onset potential was observed. The 20-junction photoelectrode showed the highest photocurrent density (−25.23 μA cm^{-2} at +0.4 V) and the most positive onset potential (+1.3 V) of all four samples. Furthermore, the 20-junction photoelectrode-based PEC exhibited a high open circuit photovoltage of up to +0.97 V, which was much higher than that reported for a cell having a single junction photoelectrode that exhibited an open circuit photovoltage of +0.13 V.[48]

The water splitting quantum efficiency of a pristine *p*-$CaFe_2O_4$ electrode was found to be relatively low, which has been assumed to be due to the poor mobility of the photogenerated charge carriers.[43] Therefore, efforts have been made to improve the conductivity of $CaFe_2O_4$ electrodes by doping the material. Doping with Na and Mg yielding oxides of the type $Ca_{1-x}Na_xFe_{2-y}Mg_yO_4$ resulted in semiconductors exhibiting higher electronic conductivity but still very small photocurrents.[43] In an attempt to improve the low quantum efficiency for the light-induced water splitting reaction, Sekizawa *et al.* have prepared various metal-doped $CaFe_2O_4$ electrodes by radio frequency magnetron co-sputtering onto glass substrates coated with antimony-doped tin oxide followed by post-annealing at a low temperature. The doping metals were aggregated in the films after annealing as revealed by scanning transmission electron microscopy. Doping of $CaFe_2O_4$ with Au and Ag resulted in an enhancement of the photocurrent without affecting the *p*-type conductivity. Doping with Ag resulted in an improvement of the carrier mobility together with a red-shift of the photoabsorption. Ag-doped $CaFe_2O_4$ showed a 23-fold higher photocurrent than undoped $CaFe_2O_4$.[49]

In a series of papers, Ida and co-authors reported about the light induced water splitting employing |*n*-semiconductor | $NaOH_{aq}$ (0.1M)||$NaOH_{aq}$ (0.1M)|*p*-$CaFe_2O_4$ based cathode | PECs.[44–46] Open-circuit voltages and short-circuit current densities of these PECs are presented in Table II. Molecular hydrogen was generated from these cells under irradiation with visible light without applying a bias (500 W Xe lamp). However, the expected H_2/O_2 ratio of 2 was not achieved (Table II) showing that O_2 evolution is suppressed and an additional suitable oxygen evolution catalyst is needed. The semiconducting materials for the photocathode were prepared by a solid state route from Fe and Ca salts varying the Fe/Ca ratio (1.8–2.1). The highest photocathodic current was observed for an electrode having a Fe/Ca ratio of 1.9, for which XRD measurements revealed the presence of $Ca_2Fe_2O_5$ as an impurity in $CaFe_2O_4$.

Yang *et al.* have investigated the photoelectrochemical performance of porous $CoFe_2O_4$ nanosheets on FTO. The electrodes have been prepared from an aqueous solution of Co and Fe nitrate via a template-free electrochemical deposition followed by a heat treatment at 933 K. The

TABLE II. Visible light induced water splitting employing | *n*-semiconductor |$NaOH_{aq}$ (0.1M) || $NaOH_{aq}$ (0.1M) | *p*-$CaFe_2O_4$ based cathode | photoelectrochemical cells.

Photoanode	Photocathode	Open-circuit voltage/V	Short-circuit current density[a]/μA cm^{-2}	H_2/O_2 ratio	References
n-TiO_2	*p*-$CaFe_2O_4$	0.97	~220	10–20	44
n-TiO_2	*p*-$CaFe_2O_4$/$Ca_2Fe_2O_5$	1.09	275	3.7	46
n-ZnO	*p*-$CaFe_2O_4$	0.82		No oxygen evolved	45

[a]Calculated from data presented in the references.

electrodes exhibited only a small cathodic photocurrent of ~0.3 μA cm^{-2} in 0.1 M aqueous Na_2S solution at zero bias voltage under visible light illumination ($\lambda \geq 390$ nm, 30 mW cm^{-2}).[51]

The photoelectrochemical properties of *p*-$NiFe_2O_4$ pellets prepared by sintering sol–gel synthesized particles at 850 °C were investigated by Rekhila *et al.* The open-circuit voltage and the short-circuit current of a |Pt|KCl(0.5M)|*p*-$NiFe_2O_4$| cell were reported to be 0.43 V and 710 μA cm^{-2} under irradiation with visible light (50 mW cm^{-2}). A photon-to-electron conversion efficiency of 0.28 was calculated. However, corrosion of the semiconductor electrode was observed under illumination as well as in the dark.[52]

Up to now, mainly PECs of the type |Pt|electrolyte|*p*-ferrite| have been studied. These cells employing ferrites as photocathodes are able to split water under visible light irradiation without applying an external bias. However, the reported photocurrents are well below those that are required for a technical application[65,66] indicating the inhibition of the interfacial charge carrier transfer.

As seldom as *p*-conducting ferrites as photocathodes, bare ferrites MFe_2O_4 with *n*-type conductivity have been investigated as photoanodes in PECs. One of the exceptions is the *n*-$ZnFe_2O_4$ electrode the photoanodic behavior of which was investigated by Wijayantha and co-workers.[53,54] The electrode was prepared by aerosol-assisted chemical vapor deposition of alcoholic solutions of a bimetallic precursor on FTO. The thickness, morphology, and nanostructure of the electrode were controlled by altering the solvent for dissolution of the bimetallic precursor and the physical deposition parameters.[53,54] The photocurrents were found to be dependent on the solvent, as well as on the deposition temperature and the deposition time. The maximum photocurrent density of 350 μA cm^{-2} at 0.44 V was obtained with a $ZnFe_2O_4$ electrode synthesized using a 0.1 M solution of the bimetallic precursor in ethanol, an optimum deposition temperature of 450 °C, and a deposition time of 35 min. This electrode showed an incident-photon-to-electron conversion efficiency of 13.5 $\times 10^{-2}$ at 350 nm and an applied potential of 0.44 V.[53] Varying the methanol/ethanol ratio of the solvent resulted in a change in the texture of the $ZnFe_2O_4$ electrode. The textured electrodes exhibited a significantly higher photocurrent under AM1.5 illumination compared to their compact counterparts. The authors attributed this behavior to the improved collection of the photogenerated minority carriers at the $ZnFe_2O_4$/electrolyte interface as the average feature size gradually decreased.[54]

In general, ferrites as photoelectrodes need high temperatures to crystallize (>1000 °C). This limits the choice of support materials and poses a critical challenge to maintain desired electrode material properties like surface area and porosity. Recently, Kim *et al.* introduced a hybrid microwave annealing (HMA) post-synthetic heat treatment with graphite powder as a susceptor which is compatible to most transparent conducting glasses. They treated solution processed β-FeOOH nanorods with a Zn nitrate solution and obtained $ZnFe_2O_4$ nanorods after thermal treatment at 550 °C for 3 h and at 800 °C for 20 min. Some unwanted ZnO on the nanorods was removed in NaOH. Subsequently, the $ZnFe_2O_4$ nanorods were subjected to HMA (5 min) to increase their crystallinity. The HMA treated $ZnFe_2O_4$ nanorods (550 °C) exhibited at +0.4 V (1M NaOH) and AM 1.5G illumination a photocurrent of 240 μA cm^{-2}, which was 10-15 fold increased in comparison to conventional thermally treated electrodes, and was stable for at least 3 h. The authors reported that stoichiometric amounts of H_2 and O_2 can be measured with Faradaic efficiencies (=actual gas evolution rate/rate expected from the current) of 90%-100%. The improved performance after the HMA treatment was attributed to better crystallinity and reduced surface defects as evinced by electrochemical impedance spectroscopy.[67]

For sometime now, the scientific interest focuses on the study of heterojunction electrodes such as the $ZnFe_2O_4/Fe_2O_3$ *n*-*n*-heterojunction[68–70] and $CaFe_2O_4/Fe_2O_3$,[71] $CaFe_2O_4$/TaON,[72] and $CaFe_2O_4/BiVO_4$[73] *p*-*n*-heterojunctions as photoanodes for the oxygen evolution reaction (OER).

Borse and coworkers have prepared $ZnFe_2O_4/Fe_2O_3$ layers on stainless steel by depositing an aqueous solution of Zn and Fe salts employing a plasma spray method and investigated the photoelectrochemical hydrogen production from water in a $|ZnFe_2O_4/Fe_2O_3|NaOH_{aq}$ (1M) |graphite| cell under simulated solar light (AM1.5G, 100 mW cm^{-2}) employing a bias of 0.6 V. Again the composite photoanode exhibited a significantly higher photoactivity than a bare $ZnFe_2O_4$ photoelectrode. The rates of HER at the $ZnFe_2O_4$ and the $ZnFe_2O_4/Fe_2O_3$ photoanodes were calculated to be 46.3 and 99.0 μmol cm^{-2} h^{-1}, respectively, resulting in solar-to-hydrogen conversion efficiencies of 0.60×10^{-2} and 1.25×10^{-2}, respectively. However, no data were given for the formation of molecular oxygen; thus, stoichiometric water splitting was not proven. The results of electrochemical impedance spectroscopy evinced a significantly lower interfacial charge transfer resistance of the $ZnFe_2O_4/Fe_2O_3$ composite electrode than of the $ZnFe_2O_4$ electrode.[68]

$ZnFe_2O_4/Fe_2O_3$ photoanodes have also been prepared via electrodeposition and chemical growth of FeOOH films on FTO and subsequent conversion into α-Fe_2O_3 by heat treatment. A Zn-containing solution was deposited on top of this α-Fe_2O_3 film yielding a Zn-rich layer at the top surface of the α-Fe_2O_3 layer after annealing.[69,70] McDonald and Choi employing the electrodeposition route obtained photoelectrodes composed of particles with an α-Fe_2O_3 (hematite) core and a $ZnFe_2O_4$ shell as confirmed by XRD. The highest photocurrent was obtained with a composite electrode exhibiting a $ZnFe_2O_4/Fe_2O_3$ ratio of 1. The increase in the photocurrent of the heterojunction electrodes compared to bare α-Fe_2O_3 electrode was claimed by the authors to be due to an enhanced electron hole separation at the $ZnFe_2O_4/Fe_2O_3$ interface. A further enhancement in photocurrent was obtained by a treatment of the composite electrodes with an Al^{3+} solution yielding thin layers of a solid solution after heat treatment. With this, probably the number of surface states that serve as electron hole recombination centers is reduced. However, it was also observed that both the formation of a $ZnFe_2O_4$ layer and the incorporation of Al^{3+} into the surface resulted in a surface being less catalytic for the OER. However, when Co^{2+} was introduced into the surface of the $ZnFe_2O_4/Fe_2O_3$ composite electrodes as oxygen evolution catalyst, the onset of the photocurrent was shifted to more negative voltage and the overall photocurrent was improved.[69]

A related photoanode has been prepared by anisotropic growth of a β-FeOOH film on FTO from an aqueous solution containing Fe and Ca ions followed by two-step thermal annealing at 550 and 800 °C. The authors assumed that this procedure induces the formation of a *p*-$CaFe_2O_4$/*n*-Fe_2O_3 heterojunction photoanode. The presence of Ca in the Fe_2O_3 film and the formation of $CaFe_2O_4$ have been evinced by XPS measurements. The photoanode showed a 100% higher photocurrent response than that obtained using a bare α-Fe_2O_3 electrode under illumination (AM 1.5G, 100 mW cm^{-2}). Based on the results of electrochemical impedance spectroscopy, the photocurrent enhancement has again been attributed to an enhanced charge carrier separation and a reduced resistance of the interfacial charge transfer between the electrolyte and the electrode.[71]

Lee and co-workers reported the preparation and characterization of *p*-$CaFe_2O_4$ modified TaON and $BiVO_4$ *p*-*n*-heterojunction photoanodes.[72,73] Both *n*-type semiconductors are known to be suitable anode materials for solar driven water splitting in PECs. The position of valence band of *p*-$CaFe_2O_4$ is more positive than the water oxidation potential, and both semiconductors, TaON and $BiVO_4$, form staggered relative band positions with the ferrite as required for an effective heterojunction photoanode. In both cases, *p*-$CaFe_2O_4$, which has been synthesized by a conventional solid state reaction, was deposited on top of the *n*-semiconductor/FTO electrode by electrophoresis. The pristine TaON electrode showed an anodic photocurrent density of 230 μA cm^{-2} at +0.42 V (0.5 M NaOH, λ >420 nm). The $CaFe_2O_4$ layer on the surface of the TaON electrode resulted in a significant increase of the photocurrent density (1260 μA cm^{-2}). The observed photocurrent was found to be the result of overall water splitting yielding H_2 and O_2 in a ratio of 1.5, however, accompanied by a deterioration of the TaON. Impedance spectroscopic analysis indicated that the formation of the heterojunction increased the photocurrent density by reducing the resistance of the charge carrier transport and, consequently, enhancing the electron-hole separation.[72] Anodic photocurrents have likewise been observed for both, $BiVO_4$ and $CaFe_2O_4/BiVO_4$ electrodes (0.5M Na_2SO_4, AM

1.5G 100 mW cm^{-2}); the bare $BiVO_4$ electrode showed a photocurrent density of 580 μA cm^{-2} at +0.82 V, while the $CaFe_2O_4/BiVO_4$ heterojunction photoanode exhibited 960 μA cm^{-2} being an increase of 65% as compared to the $BiVO_4$ electrode. The formation of the heterojunction was found to reduce the recombination of the photogenerated charge carriers on the electrode surface with little effect on the bulk recombination as evinced by an investigation of the interfacial transfer of charge carriers using hydrogen peroxide as an electron donor.[73]

The modification of the heterojunction photoanodes by depositing "cobalt phosphate" (CoPi) as an OER co-catalyst[74–79] at the surface was found to affect the photocurrent.[67,71–73]

Employing a $CoPi/CaFe_2O_4/TaON$ photoanode in 0.1 M potassium phosphate buffer solution of pH 11.5 in a three electrode system with an applied bias of ~0.55 V, total amounts of H_2 and O_2 of 123 and 59 μmol were released within 3 h of illumination with $\lambda \geq 400$ nm (500 W Hg lamp with long-pass cutoff filter) resulting in a nearly stoichiometric ratio of 2.1. The Faradaic efficiency reached ~80% for both HER and OER. The slight excess of molecular hydrogen has been attributed to the slow kinetics of oxygen evolution and the self-oxidation of TaON. However, the stability of the electrode was not optimum. The initial current decreased with time and reached about a half after 3 h. The beneficial role of the CoPi co-catalyst was revealed by performing the gas evolution experiment with a $CaFe_2O_4/TaON$ photoanode in the absence of CoPi. Under these experimental conditions, no constant photocurrent was obtained, the Faradaic efficiencies decreased (50%–70%) and the H_2/O_2 ratio became surprisingly significantly less than stoichiometric ratio (1.5:1).[72]

Similar results have been obtained with $BiVO_4$-based photoanodes. In comparison to a bare $BiVO_4$ electrode, the $CoPi/BiVO_4$ photoanode showed a higher photocurrent density. On the other hand, the $CoPi/CaFe_2O_4/BiVO_4$ electrode exhibited a lower photocurrent density when compared with the $CaFe_2O_4/BiVO_4$ heterojunction electrode, but an improved stability of the current density was observed in the presence of CoPi, indicating that the presence of the OER co-catalyst is beneficial for the stabilization of the $CaFe_2O_4/BiVO_4$ heterojunction. The evolution of H_2 and O_2 during the photoelectrochemical water splitting reaction was measured employing a three electrode $|CoPi/CaFe_2O_4/BiVO_4|$ 0.1M potassium phosphate, pH7|Pt| cell applying a bias. The total amount of H_2 and O_2 evolved within 2 h of illumination with visible light ($\lambda \geq 400$ nm) was 297 and 140 μmol, respectively. The resulting H_2/O_2 ratio of 2.1 confirmed that the generation of the photocurrent was mainly due to the water splitting reaction. The Faradaic efficiency during this reaction was reported to be about 78%–88%. The photocurrent density being initially ~4000 μA cm^{-2} dropped rapidly during the first 30 min of illumination and decreased slowly afterwards.[73]

Just as the PECs containing ferrite photocathodes, even cells with ferrite-containing photoanodes are able to split water under visible light irradiation without external bias. However, the measured photocurrents of PECs with bare ferrite photoanodes are low, again indicating the inhibition of the interfacial charge carrier transfer and, consequently, an enhanced rate of charge carrier recombination. Higher photocurrents were observed with heterojunction photoanodes due to an enhanced electron/hole separation at the interface between the two semiconductors. However, photocurrents in the order of 1000 μA cm^{-2} were only measured with efficient *n*-semiconductor electrodes having a *p*-$CaFe_2O_4$ layer on the surface. Many ferrites are known to be electrocatalysts for the OER.[80–86] Thus, cheap and varied electrode materials for PECs are a reachable target without the use of precious OER catalysts such as IrO_2 or RuO_2. It is therefore evident that more photoelectrochemical investigations employing ferrite/*n*-semiconductor heterojunctions are desirable. New synthesis routes leading to high surface area materials and low temperature processes (e.g., hybrid microwave annealing) are likely to improve the existing performance. In addition, thin underlayers or overlayers of TiO_2 and Al_2O_3 (but also of other metal oxides) are expected to enhance the photocurrent either through adjusting band alignments or by passivating surface recombination centers as it was revealed for other iron-based photoelectrodes.[87]

The conversion of solar energy into molecular hydrogen under mild operating conditions is also possible by means of photocatalytic processes.[4–8,11,12,14–17] Several semiconducting ferrites of the types MFe_2O_4 and $M_x{}^1M^2{}_yFe_{3-x-y}O_4$ have been studied as possible water splitting photocatalysts due to their ability to absorb visible light and their claimed resistance against photocorrosion.

The ability of Pt-loaded Fe_3O_4 to evolve molecular hydrogen from water-ethanol mixtures under visible light illumination was investigated by Mangrulkar *et al.* The employed single-phase

Fe_3O_4 nanoparticles were synthesized using a co-precipitation method. The reported XRD data of the synthesized compound are consistent with magnetite with spinel structure. The authors observed the evolution of molecular hydrogen in the dark at the Fe_3O_4 surface at a temperature of 100 °C (3.8 μmol h^{-1}) while no hydrogen evolved at 30 °C and 75 °C. Under illumination, an increasing temperature of the ethanol-water suspension resulted in an increasing HER rate (60 μmol h^{-1} at 85–100 °C). However, under visible light illumination at this temperature, the photocatalyst was found to be stable only up to 22 h.[88]

Magnesium ferrite, *p*-$MgFe_2O_4$, derived from layered double hydroxides (molar ratio Mg/Fe = 2), synthesized by a co-precipitation method, was found to be active for photocatalytic HER under visible light illumination (200 W lamp, 29 mW cm^{-2}). The best performance was achieved at pH 10 with a quantum efficiency of 0.5×10^{-2} in the presence of the hole scavenger Na_2SO_3 (0.025 M).[40]

Spinel $MgFe_2O_4$, orthorhombic $CaFe_2O_4$, and a bulk *p*-*n*-heterojunction photocatalyst consisting of $CaFe_2O_4$ and $MgFe_2O_4$ particles have been synthesized by Kim *et al.* employing a polymer complex method with subsequent calcination at 500–1200 °C. Single $MgFe_2O_4$ and $CaFe_2O_4$ with Pt and RuO_2 co-catalysts for the reduction and the oxidation reaction, respectively, showed only low photocatalytic activity (quantum yield QY $< 1 \times 10^{-2}$), while the co-catalysts loaded heterojunction photocatalyst consisting of both ferrites was found to be highly active for hydrogen production from a water-methanol mixture under visible light illumination (quantum yield = 10.1×10^{-2}). The HER activity was found to be higher than that of a $CaFe_2O_4/MgFe_2O_4$ photocatalyst prepared by a conventional solid-state reaction method at 1300 °C probably due to the higher crystallinity of the former.[56]

Expanding their work on the $MgFe_2O_4/CaFe_2O_4$ heterojunction photocatalyst, Kim and co-workers have investigated the effect of substitution of Fe^{3+} by Ti^{4+} in the semiconductor lattice. Again, from water-methanol mixture and under visible light illumination, the Ti^{4+} ion doped photocatalysts, $CaFe_{2-x}Ti_xO_4/MgFe_{2-x}Ti_xO_4$, with $0.01 \le x \le 0.06$, loaded with Pt as co-catalyst, showed a slightly enhanced quantum yield for this reaction (13.3×10^{-2} for $x = 0.03$) as compared to its Ti-free counterpart (10.1×10^{-2}).[89]

Visible light induced hydrogen and oxygen formation employing a $CaFe_2O_4/PbBi_2Nb_{1.9}W_{0.1}O_9$ *p*-*n*-heterojunction loaded with Pt was investigated by Kim *et al.* The authors reported a quantum yield of 38×10^{-2} for the oxygen formation in the presence of $AgNO_3$ as the sacrificial reagent under illumination with $\lambda \ge 420$ nm. The rate for hydrogen evolution from a water-methanol mixture was found to be lower than that for oxygen evolution by a factor of at least 10.[57]

Orthorhombic phase $BaFe_2O_4$ powder synthesized employing a solid state reaction was also investigated by Kim and co-workers. The ability of photocatalytic hydrogen evolution from a water-methanol mixture was tested after depositing both, Pt and RuO_2 nanoparticles on the semiconductor surface. Quantum yields of 6.24×10^{-2} and 1.73×10^{-2} were reported for the irradiation with $\lambda > 210$ nm and $\lambda > 420$ nm, respectively. Significantly lower quantum yields were calculated for only Pt-loaded $BaFe_2O_4$ showing that RuO_2 assists the charge separation.[58]

Photocatalytic hydrogen evolution induced by *p*-$NiFe_2O_4$ was studied by Peng and co-workers,[90] Hong *et al.*,[91] Kang and co-workers,[92] and Rekhila and co-authors.[52]

Peng and co-workers prepared mesoporous spinel $NiFe_2O_4$ nanoparticles via a hydrothermal process followed by calcination. Employing the spinel ferrite as the photocatalyst without any co-catalyst, they observed hydrogen evolution under visible light illumination of an aqueous suspension in absence of any sacrificial reagent. However, no evolution of molecular oxygen was detected but the pH of the reaction increased during the hydrogen evolving photoreaction. Addition of methanol into the aqueous suspension resulted in an increased hydrogen evolution rate. The pH of the suspension was found to decrease during the reaction due to the oxidation of methanol yielding formic acid. Apparent quantum efficiencies of 0.07×10^{-2} and 0.52×10^{-2} were calculated for the HER in the absence and in the presence of methanol, respectively. Increasing the calcination temperature employed during the nanoparticle synthesis resulted in increasing crystal size, but decreasing surface area and pore volume of the photocatalyst which ultimately impacts on the hydrogen evolution rate. The highest rate (~15 μmol h^{-1}) was found with nanoparticles calcined at 500 °C having a surface area of 76 m^2 g^{-1} and a total pore volume of 0.26 cm^3 g^{-1}. Samples

calcined at 300 °C and 700 °C exhibited lower rates. To evaluate the photostability of $NiFe_2O_4$, the photocatalyst was reutilized in repeated experimental runs after separation, washing, and drying. The respective amounts of molecular hydrogen formed in the second and third runs were ~96% and ~93% of the first run. Neither Ni^{2+} nor Fe^{3+} were detected in the residual solution after illumination indicating $NiFe_2O_4$ nanoparticles to be stable visible-light active photocatalysts.[90]

Hong *et al.* have synthesized submicron-sized mesoporous $NiFe_2O_4$ spheres employing an aerosol spray pyrolysis method using Pluronic F127 as the structure-directing agent. Amorphous and crystalline photocatalysts were obtained depending on the amount of the structure-directing agent and the calcination conditions. For the purpose of comparison, the authors synthesized a reference $NiFe_2O_4$ employing the above-mentioned method of Peng and co-workers. The photocatalytic performance for hydrogen evolution was examined by visible light illumination of aqueous suspensions containing methanol. The relative hydrogen evolution rates as calculated from reported rates are 1.0, 1.5, and 4.5 for the amorphous $NiFe_2O_4$ ($\geq$235 $m^2\ g^{-1}$), the reference sample (81 $m^2\ g^{-1}$), and the crystalline spinel $NiFe_2O_4$ (121 $m^2\ g^{-1}$), respectively. These data indicate that the photocatalytic activity for hydrogen evolution depends primarily on crystallinity. The surface area seems to be of secondary importance. The formation of CO_2 was observed indicating oxidation of the sacrificial reagent. Repetitive experimental runs showed no change of the HER (within experimental error) indicating the stability of the spinel photocatalysts.[91]

Kang and co-authors determined the hydrogen evolution ability of core-shell $NiFe_2O_4/TiO_2$ nanoparticles in water-methanol mixtures under UV irradiation. They prepared cubic $NiFe_2SO_4$ by a precipitation method followed by a calcination step at 500 °C. Subsequently, the spinel was coated with TiO_2 by hydrolysis of a titanium alkoxide. Molecular hydrogen was photocatalytically generated from methanolic suspensions of the core-shell nanoparticles. In contrast to the experimental results reported by Peng *et al.*[90] and Hong *et al.*[91] no hydrogen was formed from suspensions containing the bare $NiFe_2O_4$. Little conclusive, the authors argued that the enhanced hydrogen production by $NiFe_2O_4/TiO_2$ in comparison to the bare $NiFe_2O_4$ was mainly due to the effective electron/hole separation caused by the core-shell structure. Differences in the XPS spectra recorded before and after the photocatalytic reaction reveal changes in the oxidation states of the metal cations not being reversible in the time scale of the experimental runs.[92]

Rekhila *et al.* synthesized a *p*-conducting $NiFe_2O_4$ spinel photocatalyst by a sol–gel method followed by calcination at 850 °C and investigated its ability to produce molecular hydrogen from aqueous $S_2O_3^{2-}$ suspensions under visible light illumination. The amount of $NiFe_2O_4$, the pH, and the concentration of $S_2O_3^{2-}$ were varied to identify optimal reaction conditions. The highest quantum efficiency was reported to be 0.53×10^{-2}, i.e., in the range reported by others employing methanol as sacrificial agent.[52]

Yang *et al.* synthesized $CuFe_2O_4$ nanoparticles via a citric acid-assisted sol–gel method with a final calcination at 850 °C. For the purpose of comparison, $CuFe_2O_4$ materials were also fabricated by a co-precipitation method followed by calcination at 850 °C and a solid-state reaction at 1000 °C. All prepared samples exhibited tetragonal structure. The photocatalytic activity of the as-prepared photocatalysts was evaluated by measuring the amount of evolved molecular hydrogen from aqueous oxalic acid solutions under visible light illumination. Under identical experimental conditions, the highest photocatalytic HER was found using the $CuFe_2O_4$ nanoparticles synthesized via the sol–gel method. The authors did not notice a decrease of the photocatalytic HER in repeated runs (4×10 h); therefore, they concluded that $CuFe_2O_4$ is a stable photocatalyst for the photocatalytic H_2 evolution under visible light illumination.[93]

Photocatalytic, visible light induced HER with the spinel $CuFe_2O_4$ was also evaluated with alkaline suspensions containing sulfide as the sacrificial reagent. The spinel has been synthesized by solid-state reactions at $\geq$1000 °C employing a mixture of CuO and Fe_2O_3 as the reactants. A quantum yield of H_2 evolution of 0.1×10^{-2} was reported. With illumination time, the evolution of molecular hydrogen slowed down because the oxidation products competed with the adsorbed water for the light generated electrons. However, the initial performance of catalyst was almost restored using a fresh sulfite solution.[60]

The photocatalytic properties of p-$CuFe_{2-x}Mn_xO_4$ with $0 \leq x \leq 2$ with respect to hydrogen evolution from visible light illuminated suspensions containing sulfite were determined by Helaïli

TABLE III. Apparent quantum efficiency of the photocatalytic hydrogen evolution employing Cu-containing spinels.[22]

Spinel	E_g/eV	E_{fb}/V	E_{VB}/V	E_{CB}/V	$AQE/10^{-2}$
$CuFe_2O_4$	1.54	+0.11	+0.26	−1.28	0.50
$CuFe_{1.6}Mn_{0.4}O_4$	1.44	+0.16	+0.39	−1.05	1.59
$CuFe_{1.2}Mn_{0.8}O_4$	1.33	+0.16	+0.39	−0.94	0.28
$CuFe_{0.8}Mn_{1.2}O_4$	1.28	+0.32	+0.53	−0.71	0.14
$CuFe_{0.4}Mn_{1.6}O_4$	1.37	+0.32	+0.43	−0.94	0.68
$CuMn_2O_4$	1.38	+0.07	+0.18	−1.20	0.53

and co-authors. Their photocatalysts were prepared by a solid-state reaction employing appropriate amounts of CuO, Fe_2O_3, and Mn_2O_3 at 850 °C. The energetic position of the bands and consequently the bandgap energy are found to be affected by substituting Fe by Mn (Table III). All prepared spinels were photocatalytically active (Table III); the highest apparent quantum efficiency (1.59×10^{-2}) was reported for $CuFe_{1.6}Mn_{0.4}O_4$.[22]

Trari and co-workers determined the visible light induced hydrogen evolution from alkaline thiosulfate solutions in the presence of $CuFe_2O_4$ and $CuFe_2O_4/TiO_2$ as photocatalysts. $CuFe_2O_4$ was synthesized by solid state reaction of CuO and Fe_2O_3 at 850 °C, by a co-precipitation method with a final calcination step at 850 °C and by a sol–gel method with a final heat treatment at 900 °C. All the employed synthetic procedures led to the formation of tetragonal $CuFe_2O_4$. The maximum rate of H_2 evolution was found to be 15 μmol g^{-1} min^{-1} with a quantum efficiency of 1.3 %. The photocatalytic activity of the heterostructure was found to be dependent on the synthesis method of the ferrite (sol–gel reaction > solid state reaction > co-precipitation method). The authors reported that $CuFe_2O_4$ exhibits an excellent stability in alkaline media.[61]

Borse and co-authors have reported the successful photocatalytic hydrogen evolution at $ZnFe_2O_4$ surfaces.[62,64,94] Employing a water-methanol mixture and using Pt-loaded $ZnFe_2O_4$ under visible light illumination, a quantum yield of 0.15×10^{-2} was calculated. The spinel ferrite was synthesized by using the polymer complex method at the relatively low temperature of 900 °C.[62] However, also with Pt-loaded $ZnFe_2O_4$ prepared by a conventional solid-state reaction at temperatures ≥900 °C, a quantum yield of 0.11×10^{-2} was obtained under slightly different experimental conditions.[94] Iron sites in the spinel-phase $ZnFe_2O_4$ have been substituted by Ti^{4+} forming the spinels $ZnFe_{2-x}Ti_xO_4$, with $x \leq 0.08$. For the HER with Pt-loaded $ZnFe_{2-x}Ti_xO_4$ ($0.02 \leq x \leq 0.08$) from a water-methanol mixture under visible light illumination, quantum yields between 0.27×10^{-2} and 0.77×10^{-2} were reported. The highest quantum yield was obtained with $ZnFe_{1.94}Ti_{0.06}O_4$. No change of the bandgap energy of $ZnFe_2O_4$ by substituting Fe^{3+} by Ti^{4+} was observed. The authors supposed the higher electron density by *n*-type doping to be responsible for a more efficient charge separation in $ZnFe_{2-x}Ti_xO_4$ resulting in an increased photocatalytic activity.[94]

In a more recent paper, Borse and co-workers reported the synthesis of uniformly sized nanocrystalline $ZnFe_2O_4$ photocatalysts by a rapid microwave solid-state synthesis. The thus synthesized photocatalysts, possessing Brunauer-Emmett-Teller (BET) surface areas between 2.3 and 5.6 m^2 g^{-1} depending on the time of microwave irradiation, generated molecular hydrogen from a water-methanol mixture even without any loading with a co-catalyst. A maximum quantum yield of 0.19×10^{-2} at $\lambda = 420 \pm 10$ nm was determined for a material with a BET surface area of 4.6 m^2 g^{-1}. This quantum yield was approximately 3.8 times higher than that determined with a $ZnFe_2O_4$ prepared by a conventional solid-state method.[64]

Peng and co-workers have prepared a "floriated" $ZnFe_2O_4$ via a hydrothermal treatment of iron(II) and zinc(II) salts in the presence of sodium oxalate and cetyltrimethylammonium bromide followed by ion-exchange to remove the organic ions, washing, drying, and calcination at 500 °C. A "flaky" $ZnFe_2O_4$ was prepared under the same synthetic conditions without adding cetyltrimethylammonium bromide. Cubic spinel structure was confirmed by XRD for both ferrite samples. The BET surface area of the "floriated" and the "flaky" photocatalyst was reported to be 52 and 51 m^2 g^{-1}, respectively. The photocatalytic activity with respect to visible light induced HER was tested employing these photocatalysts in both, water and water-methanol mixtures. Approximately 85 μmol g^{-1} molecular hydrogen was evolved during 5 h of visible light illumination of suspensions

of the "floriated" $ZnFe_2O_4$ in water without added sacrificial reagent. However, no formation of molecular oxygen was observed leaving the question open what kind of oxidation process occurred. The pH of the suspension steadily increased from 7.3 to 9.1 during illumination. In the presence of methanol acting as sacrificial agent, 238 μmol g^{-1} molecular hydrogen was evolved under otherwise identical experimental conditions. In this case, a slight decrease of the pH from 7.5 to 7.3 was observed. This decrease was attributed to the formation of some formic acid. The evolved amount of molecular hydrogen (23.8 μmol) was found to be much lower than the theoretical value (ca. 494 μmol) calculated on the basis of the methanol reaction pathway. Although exposing almost the same surface area, the "flaky" photocatalyst exhibits significantly lower photocatalytic activity indicating lower crystallinity. No oxygen evolution in the presence of $AgNO_3$ was observed over visible light irradiated $ZnFe_2O_4$.[95]

Xu and co-workers compared the ability of the spinels $ZnFe_2O_4$, $ZnFeGaO_4$, and $ZnGa_2O_4$ to generate molecular hydrogen photocatalytically from aqueous sodium sulfite solutions under both UV-vis ($\lambda \geq 250$ nm) and visible light illumination ($\lambda \geq 420$ nm). The photocatalysts were synthesized by conventional solid-state methods at 1000 °C employing the oxides as reactants. The results of the photocatalytic experiments showed that $ZnFeGaO_4$ shows to a reasonable HER under visible light irradiation exhibiting a slightly improved performance compared with $ZnFe_2O_4$ under full range irradiation (971 *vs.* 862 μmol h^{-1} g^{-1} with $\lambda \geq 250$ nm). The authors concluded that substituting Ga into the $ZnFe_2O_4$ structure enhanced the light absorbance in the UV region and modified the electronic structure.[96]

Trari and co-workers investigated the light-induced hydrogen evolution in the presence of a $ZnFe_2O_4/SrTiO_3$ photocatalyst with $Na_2S_2O_3$ being the sacrificial agent at 50 °C. $ZnFe_2O_4$ alone was found to be an effective photocatalyst for hydrogen generation under visible illumination, but the photoactivity increased significantly when the spinel was combined with the wide bandgap semiconductor $SrTiO_3$.[63]

The ferrite photocatalysts employed for HERs in the presence of sacrificial reagents and the obtained quantum yields are summarized in Table IV. As it becomes obvious from the data given in this table, the quantum yield (defined as two times the amount of evolved molecular hydrogen divided by the number of absorbed photons) of the HER catalyzed by ferrites under illumination with visible light is usually around 1×10^{-2}. Only for $CaFe_2O_4/MgFe_2O_4$ and related *p-n*-heterojunctions, quantum yields exceeding 10×10^{-2} have been reported. It has to be mentioned that the activity of a given photocatalytically active compound seems to depend on material properties influenced by the method employed to synthesize the compound (cf. the cited papers of Hong *et al.* on $NiFe_2O_4$[91] and of Yang *et al.* on $CuFe_2O_4$[93]).

It is well known that the rate of photocatalytic hydrogen evolution depends inter alia on the amount of photocatalyst as well as on the amount of co-catalyst(s), the spectral distribution and the light intensity, the concentration of the sacrificial reagent, the pH, and the temperature of the suspension. This is of course valid also for ferrite photocatalysts.[52,61,88,93] Since it is not sure that all photocatalytic runs have been performed under optimized conditions, direct comparability of the reported quantum yields is not given. Consequently, the quantum yields tabulated in Table IV can serve only as a rough guide.

It has recently been shown that photocatalytic water splitting can be an economically attractive route if the decomposition of water is achieved stoichiometrically with a solar-to-hydrogen conversion efficiency of 10×10^{-2}.[66] This efficiency has not yet been achieved. However, $NiFe_2O_4$ is one of the few materials where photocatalytic hydrogen production under irradiation with visible light in the absence of sacrificial reagents was reported. It will be necessary to examine whether (i) the simultaneous oxygen generation becomes possible by combining $NiFe_2O_4$ with a suitable co-catalysts, and (ii) the efficiency can be improved. The data in Table IV suggest that an increase in the conversion efficiency is possible by forming heterojunctions between ferrites $M_x{}^1M^2{}_yFe_{3-x-y}O_4$ with optimized composition.

Desirable properties for semiconductors employed as electrodes in photoelectrochemical cells and as photocatalysts are narrow bandgaps near 2 eV that allow the absorption of a large part of visible solar light, suitable energetic position of the valance and the conduction bands, high conductivities, and resistance to photocorrosion in aqueous solutions. As the above summary shows, many

TABLE IV. Photocatalytic hydrogen evolution from aqueous ferrite suspensions containing sacrificial reagents.

Photocatalyst	Properties	Co-catalyst	Sacrificial reagent	Wavelength or light source	$QY/10^{-2}$	References
Fe_3O_4	Spinel (magnetite)	Pt	Ethanol	Tungsten	n. r.[a]	88
$MgFe_2O_4$	*p*, spinel	$Na_2S_2O_3$ in NaOH	Methanol	Tungsten	0.5	40
$MgFe_2O_4$	*n*, spinel	Pt and RuO_2	Methanol	$\lambda \geq 420$ nm	0.57	56
$MgFe_2O_4$	*n*, spinel	Pt	Methanol	$\lambda \geq 420$ nm	0.5	89
$CaFe_2O_4$	*p*, orthorhombic	Pt and RuO_2	Methanol	$\lambda \geq 420$ nm	0.16	56
$CaFe_2O_4$	*p*, orthorhombic	Pt	Methanol	$\lambda \geq 420$ nm	0.1	89
$CaFe_2O_4/MgFe_2O_4$	*p*-*n*-heterojunction; orthorhombic $CaFe_2O_4$	Pt and RuO_2	Methanol	$\lambda \geq 420$ nm	≤10.1 depending on preparation method	56
$CaFe_2O_4/MgFe_2O_4$	*p*-*n*-heterojunction; orthorhombic $CaFe_2O_4$	Pt	Methanol	$\lambda \geq 420$ nm	10.1	89
$CaFe_{2-x}Ti_xO_4/MgFe_{2-x}Ti_xO_4$, $0.01 \leq x \leq 0.06$	*p*-*n*-heterojunction; orthorhombic $CaFe_2O_4$	Pt	Methanol	$\lambda \geq 420$ nm	13.3–1.5 depending on x	89
$CaFe_2O_4/PbBi_2Nb_{1.9}W_{0.1}O_9$	*p*-*n*-heterojunction	Pt	Methanol	$\lambda \geq 420$ nm	n. r. (<3.8 estimated from data given in the paper)	57
$BaFe_2O_4$	Orthorhombic	Pt	Methanol	$\lambda > 210$ nm and $\lambda > 420$ nm	4.65 and <	58
$BaFe_2O_4$	Orthorhombic	Pt and RuO_2	Methanol	$\lambda > 210$ nm and $\lambda > 420$ nm	6.24 and 1.73	58
$NiFe_2O_4$	76.2 $m^2\ g^{-1}$	…	Methanol	$\lambda > 420$ nm	0.52[b]	90
$NiFe_2O_4$	Amorphous (≥235 $m^2\ g^{-1}$) and crystalline (spinel, 121 $m^2\ g^{-1}$), both mesoporous	…	Methanol	$\lambda > 420$ nm	At $\lambda = 450 \pm 10$ nm: spinel (0.0075[b]) >amorphous	91
$NiFe_2O_4$		…	Methanol	$\lambda_{max} = 365$ nm	0	92
$NiFe_2O_4/TiO_2$	Core-shell	…	Methanol	$\lambda_{max} = 365$ nm	n. r.[a]	92
$NiFe_2O_4$	*p*, inverse spinel	…	$Na_2S_2O_3$	Halogen, 50 °C	≤0.53	52
$CuFe_2O_4$	Tetragonal	…	Oxalic acid	Xe, quartz cell	n. r.[a]	93
$CuFe_2O_4$	*p*, spinel	…	K_2S in KOH	Tungsten, 50 °C	0.1	60
$CuFe_{2-x}Mn_xO_4$, $0 \leq x \leq 1.6$	*p*, spinel	…	S^{2-}	Tungsten, 50 °C	≤1.59[b] (max.: $x = 0.4$)	22

TABLE IV. (*Continued.*)

Photocatalyst	Properties	Co-catalyst	Sacrificial reagent	Wavelength or light source	$QY/10^{-2}$	References
$CuFe_2O_4$	*p*	...	$S_2O_3^{2-}$ in KOH	Tungsten, 50 °C	n. r.[a]	61
$CuFe_2O_4/TiO_2$	*p*-*n*-heterojunction	...	$S_2O_3^{2-}$ in KOH	Tungsten, 50 °C	1.3	61
$ZnFe_2O_4$	*n*, spinel	Pt	Methanol	$\lambda \geq 420$ nm	1.5	62
$ZnFe_{2-x}$ Ti_xO_4, $0 \leq x \leq 0.8$		Pt	Methanol	$\lambda \geq 420$ nm	0.11–0.77, depending on x	94
$ZnFe_2O_4$	Spinel, 2.2–5.6 $m^2\ g^{-1}$	...	Methanol	$\lambda \geq 420$ nm and solar simulator (AM 1.5)	$\lambda \approx 420 \pm 10$ nm: 0.05–0.19 depending on conditions of synthesis	64
$ZnFe_2O_4$	Spinel, porous nanorods, 51 and 52 $m^2\ g^{-1}$	...	Methanol	$\lambda > 420$ nm	n. r.[a]	95
$ZnFe_2O_4$	Spinel, 3.6 $m^2\ g^{-1}$	...	Na_2SO_3	$\lambda \geq 250$ nm and $\lambda \geq 420$ nm	n. r.[a]	96
$ZnFe_2O_4/SrTiO_3$	*p*-*n*-heterojunction	...	Na_2 S_2O_3 in NaOH	Tungsten, 50 C	n. r.[a]	63

[a]H_2 formation observed.
[b]Apparent quantum yield.

ferrites of the type MFe_2O_4 seem to fulfill these conditions since PECs containing photocathodes as well as photoanodes with a bare ferrite of the type MFe_2O_4 are able to split water under visible light irradiation without external bias. However, the reported photocurrents are well below those that are required for a technical application.[65,66] Nevertheless, the measured photocurrents of some ferrites are in the same order of magnitude as those reported for other, much more intensively studied semiconductor electrodes (cf. Table 1 in Ref. 97). The improved electrical conductivity as compared with the corresponding single component metal oxide (iron oxides) mainly attributed to the presence of different metal cations facilitating the electron transport process and/or supporting the redox chemistry at the electrolyte/semiconductor interface has significant importance in designing efficient photoelectrodes.[98]

Currently, heterostructures of different ferrites or ferrites with other semiconducting oxides show typically the best performance with respect to the measured photocurrents due to an enhanced electron-hole separation.[17] Extensive studies with electrodes made from synthetically readily accessible ferrites of the type $M_x{}^1M^2{}_yFe_{3-x-y}O_4$, are still lacking. As shown, inclusion of a third metal ion into the lattice of a ferrite MFe_2O_4 yielding $M_x{}^1M^2{}_yFe_{3-x-y}O_4$ ferrites alters the photocatalytic properties of the material. Therefore, it seems possible that a systematic investigation of these ferrites will result in electrodes having an improved performance in photoelectrochemical devices.

It has been shown that the variation of the metal ions ^1M and ^1M as well as the variation of x and y is influencing the bandgap energy, the energetic positions of the valence and of the conduction band, as well as the *p*-/*n*-semiconducting properties.

Thus, the ferrites $M_x{}^1M^2{}_yFe_{3-x-y}O_4$ seem to be a group of compounds that allows the targeted adjustment of desired material properties (bandgap engineering). Tailoring of semiconductor properties is one key to improve the performance of photoelectrochemical and photocatalytic devices. Another important aspect is the surface composition of both, normal and inverse spinel ferrites which is known to be different from their bulk composition. Low energy ion scattering (LEIS) and angle resolved XPS studies on ferrites showed that the surface is dominated by octahedral ^OM cations, while the tetrahedral ^TM cations prefer to occupy sites below the surface. These findings are of paramount importance in designing future ferrite photocatalysts since photocatalytic reactions are initiated at the electrolyte/semiconductor interface.[99,100]

This work has been funded in part by the Deutsche Forschungsgemeinschaft under the program SPP 1613 (Nos. BA 1137/13-1, BA 1137/22-1, BR 1768/9-1, WA 1116/23-1, and WA1116/28-1).

[1] A. Steinfeld, Sol. Energy **78**, 603–615 (2005).
[2] M. Roeb, M. Neises, N. Monnerie, F. Call, H. Simon, C. Sattler, M. Schmücker, and R. Pitz-Paal, Materials **5**, 2015–2054 (2012).
[3] M. Kostoglou, S. Lorentzou, and A. G. Konstandopoulos, Int. J. Hydrogen Energy **39**, 6317–6327 (2014).
[4] A. Kudo and Y. Miseki, Chem. Soc. Rev. **38**, 253–278 (2008).
[5] R. Abe, J. Photochem. Photobiol. **C 11**, 179–209 (2010).
[6] K. Maeda and K. Domen, J. Phys. Chem. Lett. **1**, 2655–2661 (2010).
[7] X. Chen, S. Shen, L. Guo, and S. S. Mao, Chem. Rev. **110**, 6503–6570 (2010).
[8] K. Maeda, J. Photochem. Photobiol. **C 12**, 237–268 (2011).
[9] S. Choudhary, S. Upadhyay, P. Kumar, N. Singh, V. R. Satsangi, R. Shrivastav, and S. Dass, Int. J. Hydrogen Energy **37**, 18713–18730 (2012).
[10] M. S. Prévot and K. Sivula, J. Phys. Chem. C **117**, 17879–17893 (2013).
[11] F. E. Osterloh, Chem. Soc. Rev. **42**, 2294–2320 (2013).
[12] A. A. Ismail and D. W. Bahnemann, Sol. Energy Mater. Sol. Cells **128**, 85–101 (2014).
[13] S. Cho, J.-W. Jang, K.-H. Lee, and J. S. Lee, APL Mater. **2**, 010703 (2014).
[14] R. Marschall, Adv. Funct. Mater. **24**, 2421–2440 (2014).
[15] T. Hisatomi, J. Kubota, and K. Domen, Chem. Soc. Rev. **43**, 7520–7535 (2014).
[16] H. Ahmad, S. K. Kamarudin, L. J. Minggu, and M. Kassim, Renewable Sustainable Energy Rev. **43**, 599–610 (2015).
[17] S. J. A. Moniz, S. A. Shevlin, D. J. Martin, Z.-X. Guo, and J. Tang, Energy Environ. Sci. **8**, 731–759 (2015).
[18] I. E. Castelli, D. D. Landis, K. S. Thygesen, S. Dahl, I. Chorkendorff, T. F. Jaramillo, and K. W. Jacobsen, Energy Environ. Sci. **5**, 9034–9043 (2012).
[19] D. Levy, V. Diella, M. Dapiaggi, A. Sani, M. Gemmi, and A. Pavese, Phys. Chem. Miner. **31**, 122–129 (2004).
[20] R. A. Candeia, M. Bernardi, E. Longo, I. Santos, and A. G. Souza, Mater. Lett. **58**, 569–572 (2004).
[21] R. A. Candeia, M. Souza, M. Bernardi, S. C. Maestrelli, I. Santos, A. G. Souza, and E. Longo, Ceram. Int. **33**, 521–525 (2007).
[22] N. Helaïli, Y. Bessekhouad, K. Bachari, and M. Trari, Mater. Chem. Phys. **148**, 734–743 (2014).
[23] E. Casbeer, V. K. Sharma, and X.-Z. Li, Sep. Purif. Technol. **87**, 1–14 (2012).

[24] Y. Matsumoto, M. Omae, I. Watanabe, and E. Sato, J. Electrochem. Soc. **133**, 711–716 (1986).
[25] Z. Šimša, P. Široký, F. Lukeš, and E. Schmidt, Phys. Status Solidi B **96**, 137–144 (1979).
[26] S. Balaji, R. K. Selvan, L. J. Berchmans, S. Angappan, K. Subramanian, and C. O. Augustin, Mater. Sci. Eng. B **119**, 119–124 (2005).
[27] K. N. Harish, H. S. B. Naik, P. N. P. Kumar, and R. Viswanath, Catal. Sci. Technol. **2**, 1033–1039 (2012).
[28] A. Manikandan, E. Hema, M. Durka, K. Seevakan, T. Alagesan, and S. A. Antony, J. Supercond. Novel Magn. **28**, 1783–1795 (2015).
[29] A. Manikandan, M. Durka, K. Seevakan, and S. A. Antony, J. Supercond. Novel Magn. **28**, 1405–1416 (2015).
[30] M. D. Archer, G. C. Morris, and G. K. Yim, J. Electroanal. Chem. **118**, 89–100 (1981).
[31] M. S. Antonious, M. Etman, M. Guyot, and T. Merceron, Mater. Res. Bull. **21**, 1515–1523 (1986).
[32] C. Ramankutty and S. Sugunan, Appl. Catal., A **218**, 39–51 (2001).
[33] R. C. C. Costa, M. F. F. Lelis, L. C. Oliveira, J. D. Fabris, J. D. Ardisson, R. R. Rios, C. N. Silva, and R. M. Lago, Catal. Commun. **4**, 525–529 (2003).
[34] R. C. C. Costa, M. F. F. Lelis, L. C. A. Oliveira, J. D. Fabris, J. D. Ardisson, R. R. V. A. Rios, C. N. Silva, and R. M. Lago, J. Hazard. Mater. **129**, 171–178 (2006).
[35] G. K. Reddy, K. Gunasekara, P. Boolchand, and P. G. Smirniotis, J. Phys. Chem. C **115**, 920–930 (2011).
[36] M. Büchler, P. Schmucki, H. Böhni, T. Stenberg, and T. Mäntylä, J. Electrochem. Soc. **145**, 378 (1998).
[37] L. G. J. de Haart and G. Blasse, Solid State Ionics **16**, 137–139 (1985).
[38] L. G. J. de Haart and G. Blasse, J. Electrochem. Soc. **132**, 2933–2938 (1985).
[39] F. A. Benko and F. P. Koffyberg, Mater. Res. Bull. **21**, 1183–1188 (1986).
[40] H. Zazoua, A. Boudjemaa, R. Chebout, and K. Bachari, Int. J. Energy Res. **38**, 2010–2018 (2014).
[41] Y. Matsumoto, M. Omae, K. Sugiyama, and E. Sato, J. Phys. Chem. **91**, 577–581 (1987).
[42] Y. Matsumoto, K. Sugiyama, and E.-I. Sato, J. Electrochem. Soc. **135**, 98–104 (1988).
[43] Y. Matsumoto, K. Sugiyama, and E.-I. Sato, J. Solid State Chem. **74**, 117–125 (1988).
[44] S. Ida, K. Yamada, T. Matsunaga, H. Hagiwara, Y. Matsumoto, and T. Ishihara, J. Am. Chem. Soc. **132**, 17343–17345 (2010).
[45] S. Ida, K. Yamada, T. Matsunaga, H. Hagiwara, T. Ishihara, T. Taniguchi, M. Koinuma, and Y. Matsumoto, Electrochemistry **79**, 797–800 (2011).
[46] S. Ida, K. Yamada, M. Matsuka, H. Hagiwara, and T. Ishihara, Electrochim. Acta **82**, 397–401 (2012).
[47] J. Cao, T. Kako, P. Li, S. Ouyang, and J. Ye, Electrochem. Commun. **13**, 275–278 (2011).
[48] J. Cao, J. Xing, Y. Zhang, H. Tong, Y. Bi, T. Kako, M. Takeguchi, and J. Ye, Langmuir **29**, 3116–3124 (2013).
[49] K. Sekizawa, T. Nonaka, T. Arai, and T. Morikawa, ACS Appl. Mater. Interfaces **6**, 10969–10973 (2014).
[50] B. T. Chang, M. Jakani, G. Campet, and J. Claverie, J. Solid State Chem. **72**, 201–208 (1988).
[51] H. Yang, Y. Mao, M. Li, P. Liu, and Y. Tong, New J. Chem. **37**, 2965–2968 (2013).
[52] G. Rekhila, Y. Bessekhouad, and M. Trari, Int. J. Hydrogen Energy **38**, 6335–6343 (2013).
[53] A. A. Tahir and K. G. U. Wijayantha, J. Photochem. Photobiol., A **216**, 119–125 (2010).
[54] A. A. Tahir, H. A. Burch, K. G. U. Wijayantha, and B. G. Pollet, Int. J. Hydrogen Energy **38**, 4315–4323 (2013).
[55] H. H. Kung, H. S. Jarrett, A. W. Sleight, and A. Ferretti, J. Appl. Phys. **48**, 2463–2469 (1977).
[56] H. G. Kim, P. H. Borse, J. S. Jang, E. D. Jeong, O.-S. Jung, Y. J. Suh, and J. S. Lee, Chem. Commun. 5889–5891 (2009).
[57] H. G. Kim, P. H. Borse, W. Choi, and J. S. Lee, Angew. Chem., Int. Ed. **44**, 4585–4589 (2005).
[58] P. H. Borse, C. R. Cho, K. T. Lim, Y. J. Lee, T. E. Hong, J. S. Bae, E. D. Jeong, H. J. Kim, and H. G. Kim, J. Korean Phys. Soc. **58**, 1672–1676 (2011).
[59] K. Dileep, B. Loukya, N. Pachauri, A. Gupta, and R. Datta, J. Appl. Phys. **116**, 103505 (2014).
[60] S. Saadi, A. Bouguelia, and M. Trari, Renewable Energy **31**, 2245–2256 (2006).
[61] A. Kezzim, N. Nasrallah, A. Abdi, and M. Trari, Energy Convers. Manage. **52**, 2800–2806 (2011).
[62] P. H. Borse, J. S. Jang, S. J. Hong, J. S. Lee, J. H. Jung, T. E. Hong, C. W. Ahn, E. D. Jeong, K. S. Hong, J. H. Yoon, and H. G. Kim, J. Korean Phys. Soc. **55**, 1472–1477 (2009).
[63] S. Boumaza, A. Boudjemaa, A. Bouguelia, R. Bouarab, and M. Trari, Appl. Energy **87**, 2230–2236 (2010).
[64] R. Dom, R. Subasri, N. Y. Hebalkar, A. S. Chary, and P. H. Borse, RSC Adv. **2**, 12782–12791 (2012).
[65] B. D. James, G. N. Baum, J. Perez, and K. N. Baum, *Technoeconomic Analysis of Photoelectrochemical (PEC) Hydrogen Production* (Directed Technologies, Inc., Arlington, VA, 2009).
[66] B. A. Pinaud, J. D. Benck, L. C. Seitz, A. J. Forman, Z. Chen, T. G. Deutsch, B. D. James, K. N. Baum, G. N. Baum, S. Ardo, H. Wang, E. Miller, and T. F. Jaramillo, Energy Environ. Sci. **6**, 1983–2002 (2013).
[67] J. H. Kim, J. H. Kim, J.-W. Jang, J. Y. Kim, S. H. Choi, G. Magesh, J. Lee, and J. S. Lee, Adv. Energy Mater. **5**, 1401933 (2015).
[68] R. Dom, G. S. Kumar, N. Y. Hebalkar, S. V. Joshi, and P. H. Borse, RSC Adv. **3**, 15217–15224 (2013).
[69] K. J. McDonald and K.-S. Choi, Chem. Mater. **23**, 4863–4869 (2011).
[70] Y. Guo, Y. Fu, Y. Liu, and S. Shen, RSC Adv. **4**, 36967–36972 (2014).
[71] M. G. Ahmed, T. A. Kandiel, A. Y. Ahmed, I. Kretschemer, F. Rashwan, and D. Bahnemann, J. Phys. Chem. C **119**, 5864–5871 (2015).
[72] E. S. Kim, N. Nishimura, G. Magesh, J. Y. Kim, J.-W. Jang, H. Jun, J. Kubota, K. Domen, and J. S. Lee, J. Am. Chem. Soc. **135**, 5375–5383 (2013).
[73] E. S. Kim, H. J. Kang, G. Magesh, J. Y. Kim, J.-W. Jang, and J. S. Lee, ACS Appl. Mater. Interfaces **6**, 17762–17769 (2014).
[74] M. W. Kanan and D. G. Nocera, Science **321**, 1072–1075 (2008).
[75] M. W. Kanan, Y. Surendranath, and D. G. Nocera, Chem. Soc. Rev. **38**, 109–114 (2009).
[76] E. M. P. Steinmiller and K.-S. Choi, Proc. Natl. Acad. Sci. U. S. A. **106**, 20633–20636 (2009).
[77] M. W. Kanan, J. Yano, Y. Surendranath, M. Dincă, V. K. Yachandra, and D. G. Nocera, J. Am. Chem. Soc. **132**, 13692–13701 (2010).

[78] Y. Surendranath, M. W. Kanan, and D. G. Nocera, J. Am. Chem. Soc. **132**, 16501–16509 (2010).
[79] G. M. Carroll, D. K. Zhong, and D. R. Gamelin, Energy Environ. Sci. **8**, 577–584 (2015).
[80] Y. Matsumoto and E. Sato, Mater. Chem. Phys. **14**, 397–426 (1986).
[81] N. K. Singh, S. K. Tiwari, K. L. Anitha, and R. N. Singh, J. Chem. Soc., Faraday Trans. **92**, 2397 (1996).
[82] R. Singh, N. Singh, and J. Singh, Electrochim. Acta **47**, 3873–3879 (2002).
[83] R. Singh, N. Singh, J. Singh, G. Balaji, and N. Gajbhiye, Int. J. Hydrogen Energy **31**, 701–707 (2006).
[84] T. Pandiarajan, S. Ravichandran, and L. J. Berchmans, RSC Adv. **4**, 64364–64370 (2014).
[85] J. Y. C. Chen, J. T. Miller, J. B. Gerken, and S. S. Stahl, Energy Environ. Sci. **7**, 1382 (2014).
[86] M. Li, Y. Xiong, X. Liu, X. Bo, Y. Zhang, C. Han, and L. Guo, Nanoscale **7**, 8920–8930 (2015).
[87] L. Steier, I. Herraiz-Cardona, S. Gimenez, F. Fabregat-Santiago, J. Bisquert, S. D. Tilley, and M. Grätzel, Adv. Funct. Mater. **24**, 7681–7688 (2014).
[88] P. A. Mangrulkar, V. Polshettiwar, N. K. Labhsetwar, R. S. Varma, and S. S. Rayalu, Nanoscale **4**, 5202–5209 (2012).
[89] P. H. Borse, J. Y. Kim, J. S. Lee, K. T. Lim, E. D. Jeong, J. S. Bae, J.-H. Yoon, S. M. Yu, and H. G. Kim, J. Korean Phys. Soc. **61**, 73–79 (2012).
[90] T. Peng, X. Zhang, H. Lv, and L. Zan, Catal. Commun. **28**, 116–119 (2012).
[91] D. Hong, Y. Yamada, M. Sheehan, S. Shikano, C.-H. Kuo, M. Tian, C.-K. Tsung, and S. Fukuzumi, ACS Sustainable Chem. Eng. **2**, 2588–2594 (2014).
[92] H. S. Kim, D. Kim, B. S. Kwak, G. B. Han, M.-H. Um, and M. Kang, Chem. Eng. J. **243**, 272–279 (2014).
[93] H. Yang, J. Yan, Z. Lu, X. Cheng, and Y. Tang, J. Alloys Compd. **476**, 715–719 (2009).
[94] P. H. Borse, J. S. Jang, J. S. Lee, F. N. Khan, M. G. Ha, J. P. Kim, J. S. Bae, E. D. Jeong, and H. G. Kim, J. Korean Phys. Soc. **59**, 2750–2755 (2011).
[95] H. Lv, L. Ma, P. Zeng, D. Ke, and T. Peng, J. Mater. Chem. **20**, 3665–3672 (2010).
[96] X. Xu, A. K. Azad, and J. T. Irvine, Catal. Today **199**, 22–26 (2013).
[97] L. M. Peter and K. G. U. Wijayantha, ChemPhysChem **15**, 1983–1995 (2014).
[98] Y. Matsumoto, J. Solid State Chem. **126**, 227–234 (1996).
[99] J. P. Jacobs, A. Maltha, J. Reintjes, J. Drimal, V. Ponec, and H. H. Brongersma, J. Catal. **147**, 294–300 (1994).
[100] I. E. Wachs and K. Routray, ACS Catal. **2**, 1235–1246 (2012).